Multiple quantum magic-angle spinning using rotary resonance excitation

Thomas Vosegaard,[a] Pierre Florian, and Dominique Massiot
Centre de Recherches sur les Matériaux à Haute Température, CNRS, 45071 Orléans Cedex 2, France

Philip J. Grandinetti[b]
Department of Chemistry, The Ohio State University, 120 W. 18th Avenue, Columbus, Ohio 43210-1173

(Received 24 July 2000; accepted 25 October 2000)

We have discovered rotary resonances between rf field strength, ω_1, and magic-angle spinning (MAS) frequency, ω_R, which dramatically enhance the sensitivity of triple quantum preparation and mixing in the multiple-quantum MAS experiment, particularly for quadrupolar nuclei having low gyromagnetic ratios or experiencing strong quadrupole couplings. Triple quantum excitation efficiency minima occur when $2\omega_1 = n\omega_R$, where n is an integer, with significant maxima occurring between these minima. For triple quantum mixing we observe maxima when $\omega_1 = n\omega_R$. In both preparation and mixing the pulse lengths required to reach maxima exceed one rotor period. We have combined these rotary resonance conditions into a new experiment called FASTER MQ-MAS, and have experimentally demonstrated a factor of 3 enhancement in sensitivity in comparison to conventional MQ-MAS. © *2001 American Institute of Physics.* [DOI: 10.1063/1.1333407]

I. INTRODUCTION

Since the introduction of multiple-quantum magic-angle spinning (MQ-MAS) (Refs. 1 and 2) for obtaining high resolution solid-state NMR spectra of quadrupolar nuclei three approaches have gained widespread use for the preparation and mixing of multiple quantum coherences. The first approach[3,4] is the use of a single pulse whose duration is much shorter than the rotor period for both preparation and mixing periods in MQ-MAS.[2,5–7] The rf field strength requirements for this approach are high, with many systems requiring field strengths of 150 kHz or greater. In addition, high MAS spinning speeds, which average away the first-order quadrupolar couplings, require even greater rf field strengths[8,9] to maintain the same excitation efficiency. A second approach, called RIACT,[10] uses an adiabatic coherence transfer between triple quantum and single quantum coherences induced by the MAS motion.[11] Once again, adiabaticity constraints often require high rf field strengths which must increase with spinning speed to maintain adiabaticity. More recently, a third approach[12–14] using fast amplitude modulation has been shown to be a more effective propagator for mixing. The mechanism for this enhancement has been explained[14] as coherence transfers induced by the adiabatic motion of the rotor,[11,15] a mechanism similar to that of RIACT,[10] but significantly more efficient. In all three approaches the need for high rf field strengths can lead to significant sensitivity problems, particularly for quadrupolar nuclei having low gyromagnetic ratios or experiencing strong quadrupole couplings.

In this letter we present a new approach for the preparation and mixing of multiple quantum coherences that exploits a rotary resonance between the rf field strength and the sample rotation under magic-angle spinning. We call this approach FAst Spinning gives Transfer Enhancement at Rotary resonance (FASTER). FASTER has an important advantage over all previous approaches that significant sensitivity gains can be found at dramatically lower rf field strengths, particularly when employing MAS probes that exploit recent technological improvements in sample spinning rates.[16]

II. EXPERIMENT

^{87}Rb MQ-MAS NMR experiments were performed at 196.367 MHz on a Bruker AVANCE-600 spectrometer and at 130.932 MHz on a Bruker DSX-400 spectrometer, both employing a MAS probe with 2.5 mm o.d. rotors. rf field strengths up to $\omega_1/2\pi = 125$ kHz were obtained on the AVANCE-600, and up to $\omega_1/2\pi = 200$ kHz on the DSX-400. rf field strengths were calibrated by measuring the pulse duration for 360° pulses for a 0.5 M aqueous solution of $RbNO_3$. Spinning frequencies were stable within ± 10 Hz. Polycrystalline $RbClO_4$ was obtained from a commercial source and used without further purification. The rotary resonance behavior outlined in this letter can be easily adapted for any of the current MQ-MAS pulse sequences[2,5–7,14,17,18] which utilize single pulse preparation and $\Delta p = \pm 2$ and ± 4 mixing.

III. RESULTS AND DISCUSSION

In the first single pulse preparation and mixing MQ-MAS experiments it was assumed that the pulse lengths were sufficiently short that the MAS time dependence in the first order quadrupolar interaction could be ignored.[2,5,7] Amoureux *et al.*,[8] however, showed that this approximation breaks down rather rapidly and within one-tenth of a rotor period significant losses in triple quantum excitation efficiency as compared to a static sample are observed. Since

[a]Present address: Laboratory for Biomolecular NMR Spectroscopy, Department of Molecular and Structural Biology, University of Aarhus, DK-8000 Aarhus C, Denmark.
[b]Author to whom correspondence should be addressed.

these sensitivity losses increase with increasing spinning speed we decided to numerically and experimentally investigate whether rotary resonance conditions exist that might recouple the first-order quadrupolar interaction, and thus improve the efficiency of multiple quantum transfer.

Employing numerical density matrix simulations of a polycrystalline sample containing spin $I=3/2$ nuclei with the quadrupolar coupling parameters $C_q=3.2\,\mathrm{MHz}$ and $\eta_q=0.21$ (i.e., those of ^{87}Rb in $RbClO_4$) we calculated the evolution of the fictitious spin half[19,20] complex observable

$$\langle \mathbf{I}_+^{1-4}(t)\rangle = \mathrm{Tr}\{\boldsymbol{\rho}(t)\mathbf{I}_+^{1-4}\} \tag{1}$$

obtained from an initial equilibrium density matrix of $\boldsymbol{\rho}_{\mathrm{eq}}=\mathbf{I}_z$ for the preparation, and the evolution of the fictitious spin half complex observables

$$\langle \mathbf{I}_\pm^{2-3}(t)\rangle = \mathrm{Tr}\{\boldsymbol{\rho}(t)\mathbf{I}_\pm^{2-3}\} \tag{2}$$

obtained from an initial density matrix of $\boldsymbol{\rho}_0=\mathbf{I}_+^{1-4}$ for the $\Delta p=-2$ and $+4$ mixing. The time dependent Hamiltonian employed in these calculations was

$$\mathbf{H}(t)=\mathbf{H}_q^{(1)}(t)+\mathbf{H}_q^{(2)}(t)+\hbar\omega_1\mathbf{I}_x\,, \tag{3}$$

where the first-order and second-order quadrupolar Hamiltonians are given by[21]

$$\mathbf{H}_q^{(1)}(t)/\hbar=\omega_q A_{2,0}(t)\mathbf{T}_{2,0}\,, \tag{4}$$

and

$$\mathbf{H}_q^{(2)}/\hbar=-\frac{\omega_q^2}{\omega_0}\sum_{k=1,2}\frac{A_{2,k}(t)A_{2,-k}(t)[\mathbf{T}_{2,k},\mathbf{T}_{2,-k}]}{k}. \tag{5}$$

A static field strength of 9.4 T, or $\omega_0/2\pi=131.364\,\mathrm{MHz}$ was employed. These calculations were performed as a function of pulse length and rf field strength for a static sample, and at various different sample spinning frequencies. All simulations were based on a full density matrix calculation and were averaged over 3722 crystallite orientations. The continuous motion of the rotor was approximated by discretizing each rotor period into 250 smaller time independent periods. A step size of 500 Hz was used when scanning through the rf field strength dimension.

Two-dimensional contour plots of the magnitude of these complex observables are shown in Figs. 1 and 3 for spinning speeds of $\omega_R/2\pi=10$, 20, 30, and 40 kHz. Above each contour plot is a skyline projection[22] onto the rf field strength axis, showing the signal maximum at each rf field strength. For comparison the skyline projection of signal maxima under static sample conditions is also shown in gray in each plot. All data are plotted using the same intensity scale for direct comparison. For the preparation this scale was set by a theoretical maximum of $|\langle \mathbf{I}_+^{1-4}\rangle|_{\max}=\mathrm{Tr}(\mathbf{I}_z\mathbf{I}_z^{1-4})=1.5$, which assumes that the triple quantum coherence created during the single pulse comes predominantly from the equilibrium polarization associated with the $m=\pm 3/2$ states. This assumption was confirmed when plots nearly identical to those of Fig. 1 were obtained using an initial density matrix of $\boldsymbol{\rho}_0=3\mathbf{I}_z^{1-4}$, that is, with the central transition ''saturated.'' In contrast, triple quantum coherence of negligible intensity was obtained when using an initial density matrix of $\boldsymbol{\rho}_0=\mathbf{I}_z^{2-3}$ in an otherwise identical calculation. Thus, in the discussions to follow the percent efficiency for triple quantum excitation will correspond to $\langle|(\mathbf{I}_+^{1-4}\rangle|/|\langle\mathbf{I}_+^{1-4}\rangle|_{\max})\times 100\%$. For the mixing we use a theoretical maximum of $|\langle\mathbf{I}_\pm^{2-3}\rangle|_{\max}=1$, which assumes complete transfer of $p=+3$ triple quantum coherence to either $p=+1$ or -1 central transition coherence. Only data for the $|\langle\mathbf{I}_-^{2-3}\rangle|$ observable (i.e., $\Delta p=-2$ mixing) is shown in Fig. 3. In regard to rotary resonance behavior the results obtained for the $\langle\mathbf{I}_+^{2-3}\rangle$ observable (i.e., $\Delta p=+4$ mixing) were nearly identical to the $\Delta p=-2$ mixing data. With these assumptions, the percent efficiency of triple quantum to single quantum mixing, in the discussions to follow, corresponds to $(|\langle\mathbf{I}_\pm^{2-3}\rangle|/|\langle\mathbf{I}_\pm^{2-3}\rangle|_{\max})\times 100\%$.

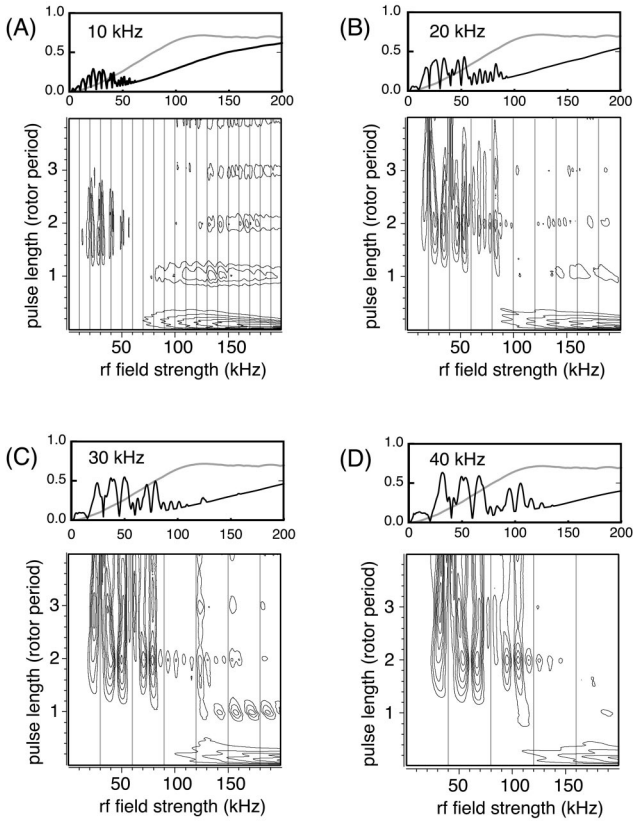

FIG. 1. Simulated two-dimensional contour plots of the magnitude of triple quantum coherence prepared as a function of pulse length and rf field strength at four different sample spinning frequencies (A) 10 kHz, (B) 20 kHz, (C) 30 kHz, and (D) 40 kHz. Equally spaced contour levels starting at 10% of $|\langle\mathbf{I}_+^{1-4}\rangle|_{\max}=\mathrm{Tr}(\mathbf{I}_z\mathbf{I}_z^{1-4})=1.5$, are shown in 5% increments. Above each contour plot is a skyline projection onto the rf field strength axis, showing the signal maximum at each rf field strength. For comparison the skyline projection of signal maxima under static sample conditions is also shown in gray.

A. Triple quantum preparation

In static samples we obtain the well known result[2,23] that the maximum triple quantum signal (shown as gray line in skyline projections of Fig. 1) is created using short pulse lengths at high rf field strengths. In this case the highest triple quantum excitation efficiency is reached in the 100–200 kHz rf field strength range and is approximately 48% of

TABLE I. Triple quantum excitation efficiency, $100\% \times (|\langle \mathbf{I}_+^{1-4} \rangle|/1.5)$, obtained at the rotary-resonance global maximum obtained for each spinning speed. The next highest rotary-resonance maximum is shown in parentheses.

$\omega_R/2\pi$ (kHz)	$\omega_1^{\max}/2\pi$ (kHz)	$\omega_1^{\max}/\omega_R$	$t_p^{\max}/T_R$	% Efficiency
10	22.0 (31.0)	2.20 (3.10)	1.7 (2.3)	19.2 (18.5)
20	53.0 (33.5)	2.65 (1.68)	2.0 (2.0)	28.8 (27.7)
30	50.0 (37.0)	1.67 (1.23)	2.0 (3.0)	36.4 (35.7)
40	31.5 (66.0)	0.79 (1.65)	3.0 (2.0)	42.2 (39.5)
50	39.0 (67.5)	0.78 (1.35)	3.0 (2.0)	49.2 (44.0)
60	46.0 (81.0)	0.77 (1.35)	3.0 (2.0)	50.8 (33.9)
70	53.0 (114.0)	0.76 (1.63)	3.0 (2.0)	47.6 (29.3)
80	60.0 (109.0)	0.75 (1.36)	3.0 (2.0)	58.3 (45.0)
90	68.0 (26.0)	0.76 (0.29)	3.0 (6.0)	44.6 (30.4)
100	74.0 (137.0)	0.74 (1.37)	3.0 (2.0)	60.4 (45.5)
110	82.0 (26.0)	0.75 (0.25)	3.0 (7.0)	49.8 (39.6)

the theoretical maximum. Considering the effect of sample rotation and focusing on the high rf field strength region of 150–200 kHz in the skyline projections of Figs. 1(A)–1(D) one sees that triple quantum excitation efficiency decreases systematically with increasing sample spinning frequency. When $\omega_R/2\pi$ reaches 40 kHz the triple quantum excitation efficiency has dropped to approximately 20% at $\omega_1/2\pi = 200$ kHz. This is consistent with the sensitivity loss under high speed MAS conditions as documented by Amoureux *et al.*[8]

On examination of the long pulse length and low rf field strength region of 0–100 kHz we observe maxima in triple quantum excitation whose positions in the ω_1 dimension scale with sample spinning speed. On this basis we assume that the mechanism for this excitation belongs to a type of rotary resonance. While we do not have a full theoretical understanding of this effect, we can discuss several noteworthy aspects apparent in Fig. 1. Most importantly, in this rotary resonance we observe minima in the triple quantum excitation when $2\omega_1 = n\omega_R$, where n is an integer. Maxima in triple quantum excitation occur between these minima. Close examination of the position of the maxima in the ω_1 dimension reveals no simple relationship for their prediction. In Table I are the positions of the global maxima in ω_1 for each spinning speed investigated. At the lowest spinning speed ($\omega_R/2\pi = 10$ kHz) the maxima occur roughly midway between the rotary resonance minima (see Fig. 1), with the global maximum of 19.2% efficiency occurring around $\omega_1/2\pi = 22$ kHz where the ω_1/ω_R ratio is 2.2. Increasing the spinning speed to $\omega_R/2\pi = 20$ kHz a global maximum of 28.8% is obtained at $\omega_1/2\pi = 53$ kHz where $\omega_1/\omega_R = 2.65$. When $\omega_R/2\pi = 30$ and 40 kHz global maxima of 36.4% and 42.2% are obtained when $\omega_1/2\pi = 50$ kHz and 31.5 kHz, i.e., at the lower ratios of $\omega_1/\omega_R = 1.67$ and 0.79, respectively. Simulations at higher, albeit currently impractical, spinning speeds reveal even greater rotary resonance enhancements. While the ω_1/ω_R ratio needed to reach the global rotary resonance maximum generally decreases with spinning speed, it does not scale continuously, but remains somewhat constant over a range of spinning speeds and then shifts discontinuously to lower values as the spinning speed increases. We also observe that the excitation efficiency at the global maximum increases with spinning speed at the lower spinning speeds and then levels off and undergoes oscillations at the higher spinning speeds. Preliminary investigations show that the optimum ω_1/ω_R ratio increases with the size of the quadrupolar coupling constant and further investigations of this dependence are in progress.

An intriguing feature of these rotary resonances is that little or no evidence of their existence begins until the pulse length exceeds one rotor period. For pulse lengths less than one rotor period one observes a monotonic increase in excitation efficiency with increasing rf field strength. The pulse lengths required to reach the enhancement maxima generally occur at or very close to two or higher integer multiples of the rotor period. Certain resonances, i.e., ω_1/ω_R values, seem to favor a specific number of rotor periods to reach the maximum. For the system considered in this study we would conclude that only pulse lengths of two or three rotor periods would need to be considered experimentally. These maxima typically fall at the top of the first oscillation of the triple quantum coherence during the pulse. The period of oscillation in the pulse length dimension is quite slow, often extending over many rotor periods, particularly at the higher spinning speeds. A Fourier transform of these oscillations reveal that the rotary resonance nutation frequencies of the triple quantum coherences are dominated by a strong narrow component at zero frequency and a broad component near 5–6 kHz in this system. The zero frequency component is quite strong, and represents a quasi-equilibrium spin-locked triple quantum state. The magnitude of this spin-locked state is smaller (about 30%–40% smaller) than the global maximum, but directly proportional to it as a function of spinning speed. The frequency of the broad component near 5–6 kHz appears to be independent of spinning speed, but is flanked on both sides by spinning sidebands at $\omega_R/2$ which diminish in intensity with increasing spinning speed. Additional calculations reveal that the frequency of this broad resonance increases with lower external field strengths. In a calculation with the second-order quadrupolar Hamiltonian omitted from the total Hamiltonian (i.e., limit of high external field strength) the broad peak becomes a broad anti-symmetric pattern centered about zero frequency with singularities around 1500 Hz. In such a limit, however, the triple quantum excitation efficiency remains relatively unchanged, indicating that this rotary resonance effect is primarily due to an interaction between the first-order quadrupolar and the rf Hamiltonians.

Given the need for pulse lengths greater than one rotor period and resonance widths in the ω_1 dimension of approximately 3 kHz in the $\omega_R/2\pi = 10$ kHz case, it is not surprising that this effect has not been observed previously at more conventional MAS rotor speeds. The excitation efficiency at rotary resonance minima drops to about 1%, and rises as high as the levels given in Table I. That these large variations can occur over such a small range of rf field strengths at the low spinning speeds implies that random fluctuations in rf field strength and/or spinning rate while in the rotary resonance regime can lead to dramatic variations in sensitivity. Thus, as in most rotary resonance experiments, a stable spinning speed and a well calibrated rf field strength are essential. The experimental advantage of these rotary resonances,

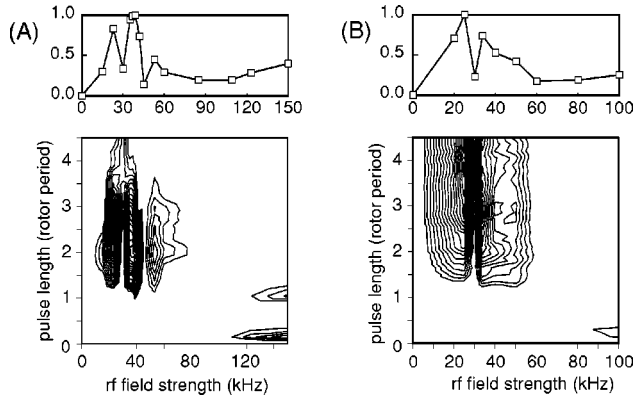

FIG. 2. Experimental two-dimensional contour plots of the magnitude of ^{87}Rb triple quantum coherence created as a function of pulse length and rf field strength in polycrystalline $RbClO_4$ spinning at $\omega_R/2\pi=30$ kHz in a static field strength of (A) 9.4 T and (B) 14.1 T. Equally spaced contour levels starting at 10% of maximum are shown in 5% increments. Above both contour plots are skyline projections onto the rf field strength axis, showing the maximum signal possible at each rf field strength. In both experiments the preparation pulse was incremented in steps of 5 μs. In (A) the mixing pulse was held constant at 0.8 μs with a rf amplitude of 200 kHz. For each point 192 scans were acquired. A selective pulse field strength 30 kHz was used for the final π pulse. In (B) the mixing pulse was held constant at 0.9 μs and a rf amplitude of 125 kHz. For each point 240 scans were acquired. A selective pulse field strength 25 kHz was used for the final π pulse.

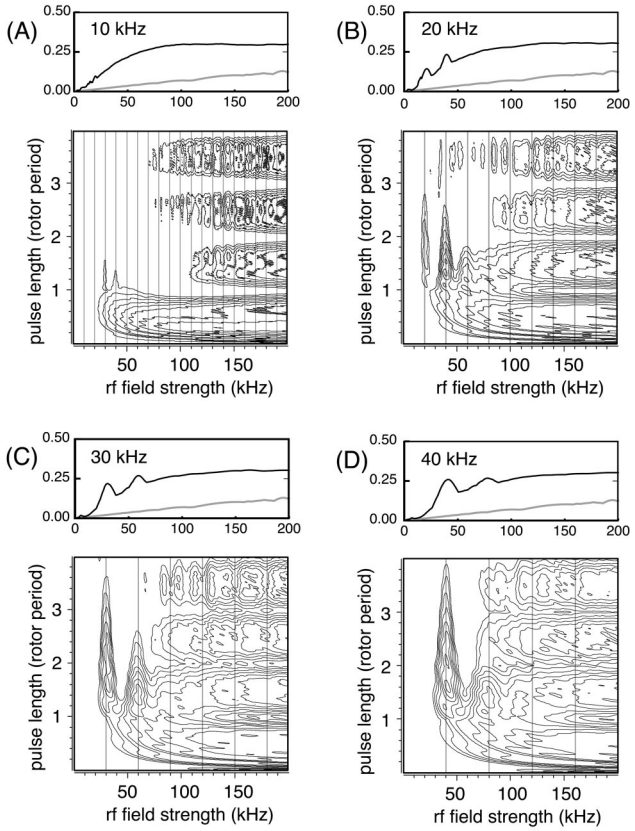

FIG. 3. Simulated two-dimensional contour plots of central transition single quantum coherence after a $\Delta p=-2$ transfer, i.e., $\boldsymbol{\rho}=\mathbf{I}_+^{1-4}\rightarrow\mathbf{I}_+^{2-3}$, as a function of pulse length and rf field strength at four different sample spinning frequencies (A) 10 kHz, (B) 20 kHz, (C) 30 kHz, and (D) 40 kHz. Equally spaced contour levels starting at 10% of $|\langle\mathbf{I}_\pm^{2-3}\rangle|_{\max}=1$, which assumes complete transfer of $p=+3$ triple quantum coherence to either $p=+1$ or -1 central transition coherence, are shown in 2.5% increments. Above each contour plot is a skyline projection onto the rf field strength axis, showing the maximum signal possible at each rf field strength. For comparison the skyline projection of signal maxima under static sample conditions is also shown in gray.

however, will be greatest at the highest possible spinning speeds. For example, at $\omega_R/2\pi=40$ kHz one would need rf field strengths well in excess of 200 kHz to match the intensity of the rotary resonance of $\omega_1/2\pi=30$ kHz. With recent advances in MAS probe technology[16] such speeds are now experimentally accessible. Thus we expect these rotary resonances will become a valuable means for efficient triple quantum coherence preparation at high spinning speeds.

To experimentally investigate this effect we employed the shifted-echo MQ-MAS sequence as outlined by Massiot *et al.*[5] and systematically varied the preparation pulse length and amplitude with the mixing pulse length and amplitude and the t_1 evolution period held constant. This experiment was performed using the ^{87}Rb signal of polycrystalline $RbClO_4$ spinning at $\omega_R/2\pi=30$ kHz. In Figs. 2(A) and 2(B) are experimental two-dimensional contour plots of triple quantum coherence created with this experiment in static field strengths of 9.4 T and 14.1 T, respectively. Additional experimental details are given in the figure caption. As predicted by numerical simulations, for pulse lengths less than one rotor period there are no rotary resonances, and instead a monotonic increase in triple quantum excitation efficiency with increasing rf field strength is observed. For pulse lengths greater than one rotor period we observe the predicted rotary resonances with the characteristic minima at $\omega_1=n\omega_R/2$. Because of instrument time constraints we were not able to explore the full shape of the rotary resonance. Between the deepest minimum and the highest maximum, however, we observe a factor of 7 enhancement.

In the 9.4 T data the maxima occur at pulse lengths near 2 rotor periods, as predicted by simulations. In the 14.1 T data, the maxima occur at pulse lengths near 3 rotor periods, revealing a slower triple quantum nutation frequency, again as predicted by the reduction in the second-order quadrupolar contribution to the Hamiltonian at higher field strengths.

B. Triple quantum mixing

A significant enhancement in multiple quantum mixing efficiency occurs when spinning the sample at the magic angle. This is clearly illustrated in the skyline projections of Fig. 3. In static samples we calculate a triple quantum mixing efficiency of approximately 12% at $\omega_1/2\pi=200$ kHz. At the same high rf field strengths but under magic-angle sample spinning the mixing is now dominated by the RIACT mechanism, with efficiencies of approximately 30% are obtained for both $\Delta p=\pm2$ and ±4 coherence transfers. (The $\Delta p=\pm3$ transfer efficiency, in contrast, is generally poor, about 10% at $\omega_1/2\pi=200$ kHz. This is achieved using short pulses, as there is no RIACT mechanism for $\Delta p=\pm3$ transfers.) One can also see the ''retreat'' of the RIACT contours towards higher rf field strengths with increasing spinning speed. At the highest rf field strengths, however, the RIACT mixing efficiency remains constant with changing spinning speed.

TABLE II. Triple quantum to single quantum mixing ($\Delta p=-2,+4$) efficiency, $100\%\times(|\langle \mathbf{I}_{\pm}^{2-3}\rangle|/0.5)$, obtained at the rotary-resonance global maximum for each spinning speed.

$\omega_R/2\pi$ (kHz)	$\omega_1^{\max}/2\pi$ (kHz)	$\omega_1^{\max}/\omega_R$	$t_p^{\max}/T_R$	% Efficiency
$10(\Delta p=-2)$	20.0	2.0	1.3	9.7
$10(\Delta p=+4)$	20.0	2.0	1.4	9.8
$20(\Delta p=-2)$	40.0	2.0	1.3	23.3
$20(\Delta p=+4)$	40.0	2.0	1.5	23.7
$30(\Delta p=-2)$	59.0	2.0	1.3	26.9
$30(\Delta p=+4)$	59.5	2.0	1.4	27.0
$40(\Delta p=-2)$	78.0	2.0	1.4	26.7
$40(\Delta p=+4)$	77.0	1.9	1.3	26.7
$50(\Delta p=-2)$	51.5	1.0	1.6	29.0
$50(\Delta p=+4)$	50.0	1.0	1.8	28.4
$60(\Delta p=-2)$	62.5	1.0	1.6	28.8
$60(\Delta p=+4)$	61.0	1.0	1.4	28.9
$70(\Delta p=-2)$	72.0	1.0	1.6	28.3
$70(\Delta p=+4)$	69.0	0.99	1.4	29.7
$80(\Delta p=-2)$	82.0	1.0	1.6	31.7
$80(\Delta p=+4)$	79.0	0.99	1.4	32.2
$90(\Delta p=-2)$	92.5	1.0	1.5	28.3
$90(\Delta p=+4)$	87.0	0.97	1.5	29.7
$100(\Delta p=-2)$	91.0	0.91	1.3	33.2
$100(\Delta p=+4)$	95.5	1.0	1.5	36.0

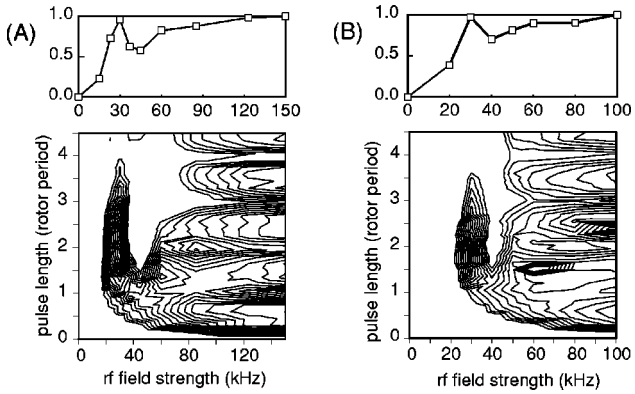

FIG. 4. Experimental two-dimensional contour plots of the magnitude of ^{87}Rb central transition single quantum coherence ($\Delta p=-2$ pathway) created from triple quantum coherence ($p=3$) as a function of pulse length and rf field strength in polycrystalline $RbClO_4$ spinning at $\omega_R/2\pi=30$ kHz in a static field strength of (A) 9.4 T and (B) 14.1 T. Equally spaced contour levels starting at 10% of maximum are shown in 5% increments. Above both contour plots are skyline projections onto the rf field strength axis, showing the maximum signal possible at each rf field strength. In both experiments the mixing pulse was incremented in steps of 5 μs. In (A) the preparation pulse was held constant at 2.0 μs with a rf amplitude of 200 kHz. For each point 384 scans were acquired. A selective pulse field strength 30 kHz was used for the final π pulse. In (B) the preparation pulse was held constant at 2.7 μs and a rf amplitude of 125 kHz. For each point 384 scans were acquired. A selective pulse field strength 25 kHz was used for the final π pulse.

On examination of the long pulse and the low rf field strength region of 0–100 kHz we again observe mixing efficiency enhancements having the characteristic behavior of rotary resonances. In contrast to the preparation rotary resonances, the mixing rotary resonances enhancements occur at $\omega_1=n\omega_R$ and provide a smaller but still significant intensity enhancement. In general, the rotary resonance line shapes in ω_1 are symmetric, and increase in width with increasing spinning speed. In contrast to the preparation rotary resonances, the variation in mixing efficiency when passing through a rotary resonance is not as dramatic, making it less sensitive to fluctuations in rotor speed and rf field strength.

In Table II are the positions of the global rotary resonance maxima in ω_1 for the $\Delta p=-2$ and $+4$ coherence transfers at each spinning speed investigated. While the rotary resonance enhancement is hardly visible at $\omega_R/2\pi=10$ kHz, it increases with spinning speed. Beyond $\omega_R/2\pi=20$ kHz the transfer efficiencies are similar to those obtained with RIACT at the higher rf field strength. Once again the ω_1/ω_R ratio needed to reach the global rotary resonance maximum increases discontinuously with increasing spinning speed, with ratios of $\omega_1/\omega_R=2$ for spinning speeds of 40 kHz or lower, and $\omega_1/\omega_R=1$ for speeds 50 kHz or greater.

As with the preparation rotary resonance, we observe a monotonic increase in mixing efficiency at pulse lengths less than one rotor period, with no rotary resonance behavior appearing until after one rotor period. The pulse lengths required to reach the rotary resonance maxima occur from 1.3 to 1.6 rotor periods, again at the top of the first oscillation in the single quantum coherence during the pulse. A Fourier transform of these oscillations show a strong narrow component at zero frequency and a broad component near 3 kHz in this system. The frequency of the broad component is independent of spinning speed, and increases with decreasing external static field strengths.

Although the rotary resonance enhancements in the mixing pulse are not as strong as in the preparation, at high spinning speeds they can still be exploited as a means of relieving rf field strength requirements without sacrificing sensitivity. At $\omega_R/2\pi=40$ kHz a rotary resonance mixing with a rf field strength of $\omega_1/2\pi=40$ kHz can provide nearly the same sensitivity as the conventional short pulse mixing with $\omega_1/2\pi=100$ kHz. Finally, there appears to be no significant difference in mixing efficiency between the $\Delta p=-2$ and $\Delta p=+4$. Thus rotary resonance mixing should be well suited for hypercomplex data acquisition, where both echo and antiecho coherence transfer pathways need to have equal transfer efficiencies.

To experimentally investigate this effect we again employed the shifted-echo MQ-MAS sequence as outlined by Massiot *et al.*[5] and systematically varied the rf amplitudes and mixing pulse lengths using the ^{87}Rb signal of polycrystalline $RbClO_4$ spinning at $\omega_R/2\pi=30$ kHz. In Fig. 4 are experimental two-dimensional contour plots of triple quantum coherence created as a function of pulse length and rf field strength for a sample of $RbClO_4$ spinning at $\omega_R/2\pi=30$ kHz in a static field strength of 9.4 T and 14.1 T. Additional details are given in the figure caption. As predicted the mixing contour plots shows three regions of maximum efficiency: (1) the traditional regime of high efficiency using high rf field strengths and short pulse lengths, (2) the RIACT regime of high efficiency using high rf field strengths and pulse lengths of approximately one or two thirds of a rotor period, and (3) the rotary resonance regime at low rf field

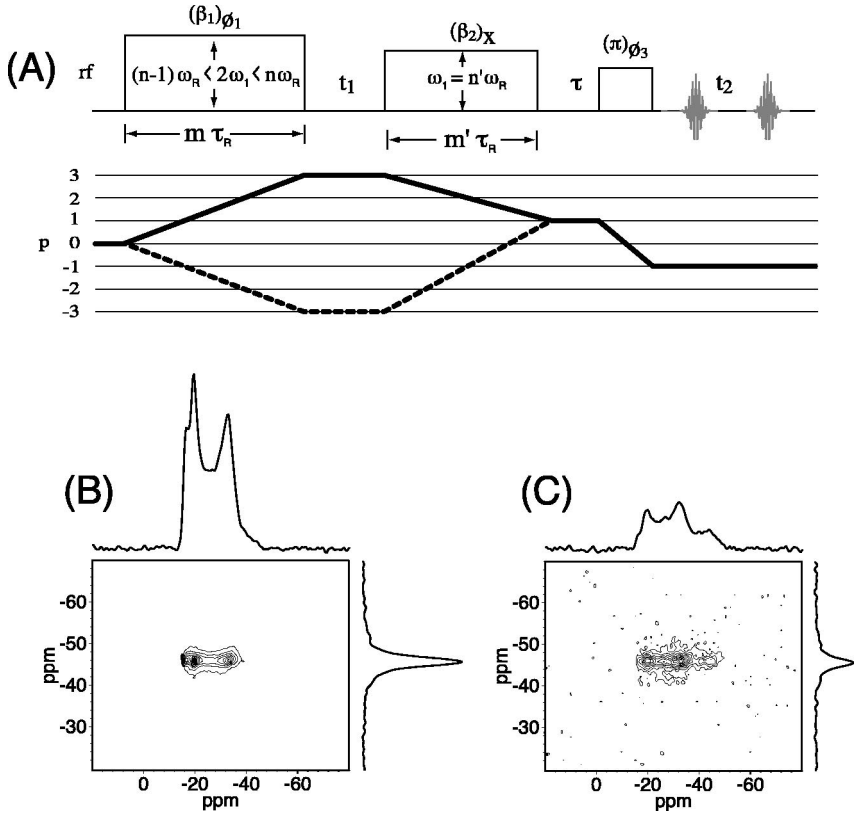

FIG. 5. (A) FASTER MQ-MAS sequence for exploiting rotary resonance sensitivity enhancement. The rf field strength of the first (preparation) pulse is adjusted to be approximately midway between the rotary resonance conditions $\omega_1 = n\omega_R/2$, and the second (mixing) pulse is adjusted to the rotary resonance condition $\omega_1 = n\omega_R$. Other than variations in rf field strength and pulse length the sequence and subsequent data processing is identical to that presented in Massiot *et al.* (Ref. 5). Phase cycle for hypercomplex acquisition is also identical to that given by Eqs. (18) and (19) in Massiot *et al.* (Ref. 5). In (B) and (C) are two-dimensional ^{87}Rb multiple quantum spectra of $RbClO_4$ comparing performance of the FASTER MQ-MAS sequence to the conventional MQ-MAS sequence, respectively. Both experiments were performed by acquiring $t_1 \times t_2 = 128 \times 256$ points using a dwell time (Ref. 24) of 66.67 μs in t_1 and 20 μs in t_2. In addition, a selective pulse field strength of $\omega_1/2\pi = 30$ kHz was used for the final π pulse and 120 scans were acquired in both experiments. A preparation pulse with $\tau_p = 75$ μs (2.25 rotor periods) and $\omega_1/2\pi = 37$ kHz and a mixing pulse with $\tau_m = 65$ μs (1.95 rotor periods) and $\omega_1/2\pi = 30$ kHz were used in the FASTER experiment. Both spectra were recorded at 9.4 Tesla. In the conventional MQ-MAS spectrum a preparation pulse with $\tau_p = 2.0$ μs and $\omega_1/2\pi = 200$ kHz and a mixing pulse with $\tau_m = 0.8$ μs and $\omega_1/2\pi = 200$ kHz were used. The sensitivity enhancement obtained with FASTER MQ-MAS is approximately a factor of 3.

strengths with maxima at $\omega_1 = n\omega_R$ with pulse lengths longer than one rotor period.

In both the 9.4 Tesla and 14.1 Tesla experiments the global rotary resonance maximum occurs at the $\omega_1/\omega_R = 1$ ratio instead of the predicted $\omega_1/\omega_R = 2$ ratio, and at pulse lengths closer to 2 rotor periods instead of the shorter pulse lengths. These differences, however, are not significant given the small difference in the predicted enhancements with the two ratios, and the broad maxima in the pulse length dimension due to the slow single quantum oscillations. Most importantly, we see experimentally that rf field strengths near $\omega_1/2\pi = 100$ kHz are required in the RIACT regime to match the sensitivity obtained with $\omega_1/2\pi = 30$ kHz in the rotary resonance regime.

C. FASTER MQ-MAS

We have combined the rotary resonance conditions described above for the preparation and mixing of multiple quantum coherence into a MQ-MAS sequence called FASTER (FAst Spinning gives Transfer Enhancement at Rotary resonance) MQ-MAS. In this sequence the rf amplitude of the preparation pulse is optimized by adjusting its amplitude to find the global maximum between the rotary resonance minima at $2\omega_1 = n\omega_R$, and the mixing pulse amplitude is adjusted to the rotary resonance condition $\omega_1 = n\omega_R$. The pulse lengths for the preparation and mixing are greater than one rotor period. For the preparation they are set to approximately two or three rotor periods, and for the mixing will typically need to be optimized to somewhere within one to three periods. In Figs. 5(B) and 5(C) are two-dimensional ^{87}Rb multiple quantum spectra of $RbClO_4$ comparing performance of the FASTER MQ-MAS sequence to the conventional single pulse preparation and mixing MQ-MAS sequence using the highest rf power possible, i.e., $\omega_1/2\pi = 200$ kHz in this case. Additional experimental details are given in the caption of Fig. 5. The sensitivity enhancement obtained with FASTER MQ-MAS is approximately a factor of 3 better. In addition to the sensitivity enhancement, FASTER MQ-MAS also provides a simple experimental protocol with preparation and mixing pulse lengths set to integer multiples of the rotor period. Moreover, the preparation and mixing pulse amplitudes are constrained by the spinning speed, and one only needs to determine which rotary resonance condition is optimal. While FASTER

MQ-MAS will lead to optimum sensitivity, it still suffers from the limitation, as with other MQ-MAS sequences, that the integrated intensities are dependent on quadrupolar coupling parameters. Thus extracting site populations can be problematic. Determining the overall transfer efficiency for sites with different couplings may require full density matrix simulations taking all NMR parameters in account. Finally, we note that the anisotropic line shapes obtained with FASTER MQ-MAS are distorted, as they are with RIACT MQ-MAS, due to varying excitation efficiencies among different crystallite orientations.

IV. CONCLUSIONS

Through numerical density matrix simulations and experimental measurements we have discovered rotary resonances between the rf field strength and the MAS frequency that can be used to dramatically enhance the sensitivity of the triple quantum preparation and mixing in the MQ-MAS experiment, particularly for those having low gyromagnetic ratios or experiencing strong quadrupole couplings. We believe this advance opens significant new possibilities for solid-state NMR of quadrupolar nuclei. For triple quantum preparation we observe minima in the excitation efficiency when $2\omega_1 = n\omega_R$, where n is an integer, and maxima between these minima. An intriguing feature of both the preparation and mixing resonances is that they do not occur until the pulse length exceeds one rotor period. The preparation pulse lengths required to reach these resonances occur at integer multiples of the rotor period and must be greater than one rotor period. For triple quantum to single quantum mixing we observe maxima in the mixing efficiency when $\omega_1 = n\omega_R$. The mixing pulse lengths required to reach these resonances are also greater than one rotor period. We have combined these rotary resonance conditions into an experiment called FASTER MQ-MAS. In an experimental comparison of MQ-MAS sensitivities using FASTER with conventional high power short pulse preparation and mixing we obtained a factor of 3 enhancement in sensitivity. The experimental setup for FASTER MQ-MAS is simple, with optimum rf amplitudes constrained by the sample spinning frequency and the pulse lengths typically set to integer multiples of the rotor period. Preliminary investigations have shown that these ideas can be extended to higher spin nuclei, and further work along these lines is also in progress.

ACKNOWLEDGMENTS

P.J.G. acknowledges support by a grant from the National Science Foundation (No. CHE-9807498). We thank Professor G. Bodenhausen for access to high field facility at ENS Paris, France, and Dr. Hans Forster, Bruker GmbH, Karlsruhe, Germany for the loan of a high-speed MAS probe, and the Ohio Supercomputer Center. Financial support from EEC ARI Contract No. NPRI-CT-1999-00042, CNRS, and Région Center is acknowledged. T.V. acknowledges financial support from the Carlsberg Foundation.

[1] L. Frydman and J. S. Harwood, ''Isotropic spectra of half-integer quadrupolar spins from bidimensional magic-angle spinning NMR,'' J. Am. Chem. Soc. **117**, 5367 (1995).
[2] A. Medek, J. S. Harwood, and L. Frydman, ''Multiple-quantum magic-angle spinning NMR: A new method for the study of quadrupolar nuclei in solids,'' J. Am. Chem. Soc. **117**, 12779 (1995).
[3] S. Vega and A. Pines, ''Operator formalism for double quantum NMR,'' J. Chem. Phys. **66**, 5624 (1977).
[4] S. Vega, T. W. Shattuck, and A. Pines, ''Fourier-transform double-quantum NMR in solids,'' Phys. Rev. Lett. **37**, 43 (1976).
[5] D. Massiot, B. Touzo, D. Trumeau, J. P. Coutures, J. Virlet, P. Florian, and P. J. Grandinetti, ''Two-dimensional magic-angle spinning isotropic reconstruction sequences for quadrupolar nuclei,'' Solid State Nucl. Magn. Reson. **6**, 73 (1996).
[6] G. Wu, D. Rovnyak, B. Sun, and R. G. Griffin, ''High-resolution multiple quantum MAS NMR spectroscopy of half-integer quadrupolar nuclei,'' Chem. Phys. Lett. **249**, 210 (1996).
[7] C. Fernandez and J. P. Amoureux, ''Triple-quantum MAS-NMR of quadrupolar nuclei,'' Solid State Nucl. Magn. Reson. **5**, 315 (1996).
[8] J. P. Amoureux, M. Pruski, D. P. Lang, and C. Fernandez, ''The effect of rf power and spinning speed on MQ-MAS NMR,'' J. Magn. Reson. **131**, 170 (1998).
[9] F. H. Larsen and N. C. Nielsen, ''Effects of finite RF pulses and sample spinning speed in multiple-quantum magic-angle spinning (MQ-MAS) and multiple-quantum quadrupolar carr-purcell-meiboom-gill magic-angle spinning (MQ-QCPMG-MAS) nuclear magnetic resonance of half-integer quadrupolar nuclei,'' J. Phys. Chem. A **103**, 10825 (1999).
[10] G. Wu, D. Rovnyak, and R. G. Griffin, ''Quantitative multiple-quantum magic-angle spinning NMR spectroscopy of quadrupolar nuclei in solids,'' J. Am. Chem. Soc. **118**, 9326 (1996).
[11] A. J. Vega, ''MAS NMR spin locking of half-integer quadrupolar nuclei,'' J. Magn. Reson. **96**, 50 (1992).
[12] A. P. M. Kentgens and R. Verhagen, ''Advantages of double frequency sweeps in static, MAS, and MQMAS NMR of spin $I=3/2$ nuclei,'' Chem. Phys. Lett. **300**, 435 (1999).
[13] P. K. Madhu, A. Goldbourt, L. Frydman, and S. Vega, ''Sensitivity enhancement of the MQ-MAS NMR experiment by fast amplitude modulation of the pulses,'' Chem. Phys. Lett. **307**, 41 (1999).
[14] P. K. Madhu, A. Goldbourt, L. Frydman, and S. Vega, ''Fast radio-frequency amplitude modulation in multiple-quantum magic-angle spinning nuclear magnetic resonance: Theory and experiments,'' J. Chem. Phys. **112**, 2377 (2000).
[15] J. H. Baltisberger, S. L. Gann, P. J. Grandinetti, and A. Pines, ''Cross-polarization dynamic-angle spinning nuclear magnetic resonance of quadrupolar nuclei,'' Mol. Phys. **81**, 1109 (1994).
[16] A. Samoson and T. Tuherm, Faster MAS, The Alpine Conference on Solid State NMR, Chamonix, France, September 1999.
[17] J. P. Amoureux, C. Fernandez, and S. Steuernagel, ''Z filtering in MQ-MAS NMR,'' J. Magn. Reson., Ser. A **123**, 116 (1996).
[18] T. Vosegaard, F. H. Larsen, H. J. Jakobsen, P. D. Ellis, and N. C. Nielsen, ''Sensitivity-enhanced multiple-quantum MAS NMR of half-integer quadrupolar nuclei,'' J. Am. Chem. Soc. **119**, 9055 (1997).
[19] S. Vega, ''Fictitious spin-1/2 operator formalism for multiple quantum NMR,'' J. Chem. Phys. **68**, 5518 (1978).
[20] A. Wokaun and R. R. Ernst, ''Selective excitation and detection in multilevel spin systems: Application of single transition operators,'' J. Chem. Phys. **67**, 1752 (1977).
[21] M. Goldman, P. J. Grandinetti, A. Llor, Z. Olejniczak, J. R. Sachleben, and J. W. Zwanziger, ''Theoretical aspects of higher-order truncations in solid-state NMR,'' J. Chem. Phys. **97**, 8947 (1992).
[22] R. R. Ernst, G. Bodenhausen, and A. Wokaun, *Principles of Nuclear Magnetic Resonance in One and Two Dimensions* (Oxford University Press, Oxford, 1987).
[23] J. P. Amoureux, C. Fernandez, and L. Frydman, ''Optimized multiple-quantum magic-angle spinning NMR experiments on half-integer quadrupoles,'' Chem. Phys. Lett. **259**, 347 (1996).
[24] D. Massiot, ''Sensitivity and line shape improvements of MQ-MAS by rotor-synchronized data acquisition,'' J. Magn. Reson., Ser. A **122**, 240 (1996).